# Identification of magnetic induced strain of electrical steels using non-destructive acceleration measurement and inverse vibration modeling

E. Salloum, O. Maloberti, S. Panier, M. Nesser, P. Klimczyk, J. Fortin

Version of Record: https://www.sciencedirect.com/science/article/pii/S0022460X20306350
Manuscript_a60471c60c76cdda4201880bfed943d4

# Identification of Magnetic Induced Strain of Electrical Steels Using Non-Destructive Acceleration Measurement and Inverse Vibration Modeling

E. Salloum[a], O. Maloberti[a,b], S. Panier[a], M. Nesser[a], P. Klimczyk[c] and J. Fortin[a,b]

[a] *Laboratoire des Technologies Innovantes, LTI-EA 3899, Université de Picardie Jules Verne, Amiens 80025, France*
[b] *ESIEE Amiens, 14 quai de la Somme BP10100, Amiens 80082, France*
[c] *Dr. Brockhaus Messtechnik GmbH and Co. KG, Lüdenscheid, Germany*

ARTICLE INFO

*Keywords*:
Non-destructive measurement
Inverse Methods
Vibration
Single Sheet Tester
Magnetostriction
Piezoelectric accelerometer
Resonance frequency
Finite element method (FEM)
Magneto-mechanical coupling
Harmonics

Abstract

Magnetic induced strain is an important source of vibration in electromagnetic components and electrical machines. This magneto-mechanical behavior is identified using a non-destructive experimental technique that consists in measuring in a Single Sheet Tester the time dependent acceleration at the free end of a fixed-free magnetic sheet and its corresponding magnetic field and induction signals. The determination of this property in the longitudinal direction is investigated using an inverse application of the longitudinal vibration equation. The strain dependence on the exciting frequency as function of the resonance frequency is also evaluated. The apparent strain that includes the inertia effect is distinguished from the magnetic-induced strain. Both strains are identified and analyzed for different frequencies lower and higher than the sample's natural frequency. We also investigated the effect of excitation's harmonics on the mechanical response.

## 1. Introduction

This papers presents an experimental procedure to identify the magnetic induced strain in soft magnetic materials. This magneto-mechanical effect measurable at the macroscopic scale is due to the microscopic intrinsic magnetostriction effect in magnetic materials [1]. In fact, magnetostriction is an important source of vibration and noise in electromagnetic components such as transformers, inductors or electrical machines. It is widely considered by researchers and its contribution in the noise generation is largely studied [2, 3, 4, 5, 6, 7]. Magnetostriction is defined by the local strain of a medium subjected to a magnetic field [8]. In fact, the application of a magnetic field in electrical steels generates the rotation of magnetic domains and the displacement of magnetic walls in the domain structure. This induces a deformation of the domains called magnetostriction and eventually the deformation of the grains containing this domains.

One of the main challenges is to understand the relationship between this mechanical behavior and the magnetization. For this, an identification technique of the magneto-mechanical behavior must first be adopted. The identification of the magnetostriction in electrical steels requires both modeling and measurement of the magneto-mechanical behavior. Model based on the Helmholtz free energy can couple statistically magnetic to mechanical behavior [1, 9, 10, 11, 12]. Mudivarthi et al. [13] studied the magneto-mechanical coupling based on energy minimization at the domain's scale. As for the measurement, strain gauges are mainly used to determine the local deformation in both longitudinal and transverse directions [14, 15, 16, 17]. Another technique, the heterodyne laser interferometry, is adopted to measure the magnetostriction [18]; it is less disturbed by noise than strain gauges. This technique is also used to measure the elastic modulus based on the resonance and anti-resonance frequencies [19, 20]. Another measurement technique uses accelerometers instead of strain gauges and requires a new experimental setup [21, 22].

* This work was carried out within the frame of the project ESSIAL, funding from the European Union's Horizon 2020, research and innovation program under grant agreement No 766437.

*Corresponding author
salloum.elias@u-picardie.fr (E. Salloum)
www.u-picardie.fr (E. Salloum)
ORCID(s): 0000-0003-1397-2741 (E. Salloum)

This paper covers the identification of magnetostriction in grain-oriented electrical steels using a piezoelectric accelerometer. It is considered as a macroscopic local strain due to the magnetization process and that eventually includes microscopic phenomena at magnetic domains scale. An experimental procedure is performed inside the Single Sheet Tester (SST); a uniform magnetic field is applied parallel to the surface of the magnetic sample in the longitudinal direction. A piezoelectric accelerometer is used for measurement of the acceleration's time response at the free end of the fixed-free sample in parallel with the magnetic measurement. This setup is a non-destructive experimental technique that provides an homogenized analysis by calculating the magnetic induced strain that is averaged through the whole structure. Based on the measured acceleration signal, the strain is identified using an inverse method of the longitudinal vibration equation. Two equivalent identified strains are distinguished; the apparent strain that includes the inertia effect and that characterizes the noise and vibration for a specific geometric configuration, and the magnetic induced strain that excludes the inertia effects and characterizes the intrinsic magneto-mechanical behavior. The frequency dependence on the identified strains is also developed.

## 2. Magnetostriction and Magnetic-Inducted Strain

At the microscopic scale, magnetic materials are constituted of magnetic domains oriented each in a specific direction. Even if the material is not globally magnetized, each magnetic domain is magnetized in different orientation in a way that the sum of the different magnetization vectors is equal to zero in a grain. The non-magnetized state has also an initial deformation. When a magnetic field is applied in a specific direction, the material begins to magnetize by promoting the increase of the domains size which orientation is parallel to the applied magnetic field and decreasing the domains size that are in the opposite direction. In general, when no mechanical stress is applied, a magnetic induced strain called magnetostriction increases in the same direction of the magnetic field and decreases in the transverse direction. Fig. 1 illustrates the magnetization and the deformation of a grain constituted of 4 magnetic domains: 2 of them are horizontally oriented in an opposite orientation (180° domains) and 2 others are vertically oriented also in an opposite direction each (90° domains). This deformation generates a magnetic induced strain $\epsilon_{ms}$ at the macroscopic scale.

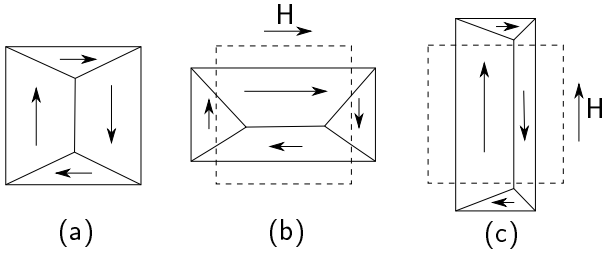


**Figure 1**: Stress-free magnetostriction generation in the domain structure with (a) No magnetic field applied (b) Magnetic field applied parallel to the 180° domains (c) Magnetic field applied parallel to the 90° domains. - - - Before magnetization, —— After magnetization.

## 3. Magneto-Mechanical Measurement Procedure

### 3.1. Magnetic Setup

The proposed experiments are performed in the SST illustrated in Fig. 3. This apparatus, designed by "Dr. Brockhaus Messtechnik GmbH & Co. KG Company" for magnetic measurement of iron losses and the hysteresis, provides time dependent signals of the average induction $B(t)$ versus the uniform surface magnetic field $H(t)$ by measuring respectively the voltage in the secondary coils system and the current in the primary coils [23]. In fact, the secondary voltage is digitally or analog controlled to obtain the user defined amplitude of sinusoidal polarization/induction at a specific magnetic field. Measurements are performed in a 1-D longitudinal direction parallel to the applied magnetic field, considered as the principal magnetization direction. The magnetic measurements are supposed uniform in this direction and on the magnetized zone of the sample. However, the local magnetic field and induction vary in the cross

section ($z-$ direction):

$$B(t) =< B(z,t) >= \frac{1}{h}\int_{\frac{-h}{2}}^{\frac{h}{2}} B(z,t)dz \tag{1}$$

The average induction $B(t)$ measured in the SST is horizontally directed ($x-$direction). However, for a Grain-Oriented sheet, induction components are also obtained in the other direction due to the material's magnetic anisotropy. These directions are not considered in this study because the tester's limitations are in the $x$ direction. Therefore, a one dimensional analysis of the strain is performed in the SST.

### 3.2. Strain gauges vs Accelerometers for Mechanical Measurements

Strain measurement is sensitive to any disturbance in the experimentation. In fact, the use of strain gauges needs special bonding skills on the sheet's surface, otherwise the collected data contain noise and disturbance [18]. In addition, strain gauges are single-use components and require a large bonding surface, and once removed, bonding is left on the surface, not to forget the sensitivity to sheet's surface coating and the time consumption that requires the wires welding.

Due to those disadvantages, a piezoelectic accelerometer (Fig. 2) is used instead of strain gauges. The sensors are provided by"DJB instruments", that are easily bonded on the surface and that can be reused on the other sheets which constitutes a non-destructive testing technique.

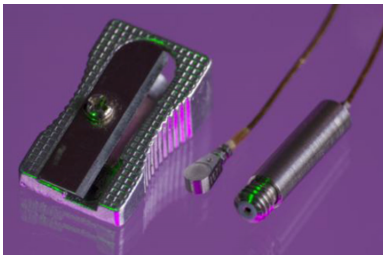

**Figure 2**: Piezoelectric accelerometer used for measurement (voltage sensitivity= 1 mV/g).

### 3.3. Mechanical Setup

The average strain generated from the magnetization is calculated from the measured acceleration. Therefore, the SST requires some modifications regarding the boundary conditions in a way to measure the acceleration and determine the strain in the longitudinal direction with the simplest possible model. Therefore, the upper yoke is removed and the sample is clamped at one end on a fixture frame and free at the other end where a piezoelectric accelerometer is bonded in order to measure the transient response of the global longitudinal acceleration signal $a(t)$ [21]. A non-magnetic plate is placed under the magnetic sheet in the magnetized region in order to prevent the friction and the out of plane vibration coming from the yoke poles. In parallel, the mean induction $B(t)$ and the surface magnetic field $H(t)$ signals are determined synchronously with the acceleration (Fig. 6). Eventually, the magneto-mechanical signals are collected inside a specific amplifier and integrated in a computer for data acquisition using a dedicated software (Catman). The global experimental setup is illustrated in Fig. 3.

### 3.4. Discrepancy Analysis

Since the experimental magneto-mechanical setup has just been designed, a discrepancy analysis is considered to evaluate the measurements accuracy and precision. First, measurements are repeated 7 times for the same experimental conditions with specific induction amplitudes (0.5 T, 1 T and 1.5 T) and exciting frequencies (250 Hz, 500 Hz, 1,500 Hz and 3,000 Hz). The accuracy calculation is obtained by repeating the same measurement without changing any experimental condition. It shows a maximal discrepancy of 2.5 % between the difference repeated measurements.

Next, a precision analysis is performed to study the sensitivity of the experimental conditions (clamping force, sensor's bonding, plate's positionning) on the certainty of the results. The experimental procedure is repeated by applying and removing the clamping at the first end and by bonding and removing the accelerometer at the other end. Results are

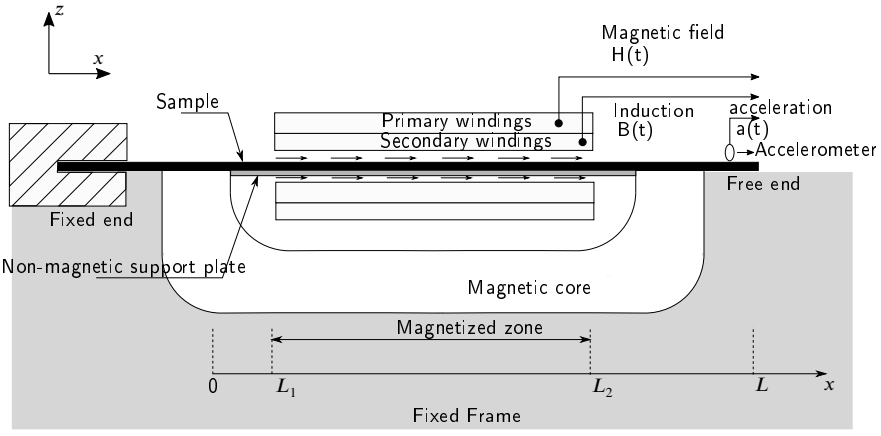


**Figure 3**: Experimental setup.

illustrated in Fig. 4 for (1 T, 3,000 Hz), and in Table 1 for different induction magnitudes and frequencies. The maximal discrepancy due to the precision is much higher than the accuracy error, reaching 9%.

| Frequency (Hz) | Induction (T) | Total discrepancy (%) |
|---|---|---|
| 250 Hz | 1 T | 3.18% |
| 250 Hz | 1.5 T | 4.76% |
| 1,500 Hz | 0.5 T | 2.99% |
| 1,500 Hz | 1 T | 2.22% |
| 3,000 Hz | 0.5 T | 9.08% |
| 3,000 Hz | 1 T | 9.91% |

**Table 1**
Dispersion due to the reproducibility on the measured acceleration.

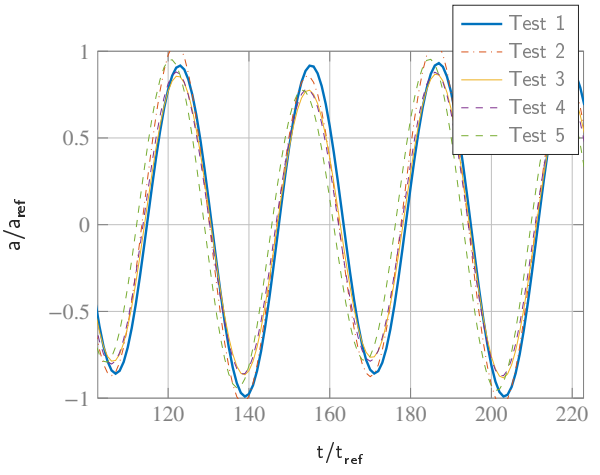


**Figure 4**: Reproducibility measurements at (1 T, 3,000 Hz).

## 3.5. Signal Resampling

Measured signals are collected with a maximal sampling frequency of 38,400 Hz. This frequency respects the Nyquist-Shannon Sampling Theorem, considering that the highest signal frequency reaches 6,000 Hz. However, the

higher the exciting frequency is, the worse the signal becomes. For example, at 1,500 Hz magnetic frequency a mechanical response is obtained at 3,000 Hz, corresponding to 38,400 / 3,000 ≈ 13 samples per cycle (Fig. 5). This information is acceptable as long as no integration is needed. However, the derivation of the strain as explained later on requires a double integration of the acceleration signal and the induction requires a simple integration of a voltage signal. Therefore, a resampling of the signals is performed with smaller time sampling size (Fig. 5). Considering the sampled signal $a_1[n], n = 1, 2, ..., N$ with $N$ samples and a sampling frequency $F_s$, the Discrete Fourier Transform $A_1[k], (k = 1, 2, ...N - 1)$ of $a_1[n]$ at a frequency $f$ is given by:

$$A_1[k] = \sum_{n=0}^{N-1} a_1[n] e^{\frac{-2\pi jkn}{N}} \tag{2}$$

where $n$ is the index of the signal $a_1$ for a specific time $t_n = n/F_s$, and $k$ is the index of the frequency signal $A_1$ for a specific frequency $f$ where $k = \frac{Nf}{F_s}$ and $0 \leq f \leq \frac{N-1}{N} F_s$. Now we consider $a_2$ the resampled signal of $a_1$ with a sampling frequency $\alpha F_s$ where $\alpha$ is the sample frequency amplification. The $\alpha N$ samples of $a_2$ are determined by the Inverse Discrete Fourier Transform of $A_1$,

$$a_2[n] = \sum_{k=0}^{K} A_1[k] e^{\frac{2\pi jkn}{\alpha N}} \tag{3}$$

Based the Nyquist-Shannon Theorem, $K$ is chosen in a way that to cancel in $a_1$'s spectrum the contribution of frequencies that are higher than $F_s/2$. Therefore, $K = (N - 1)/2$.

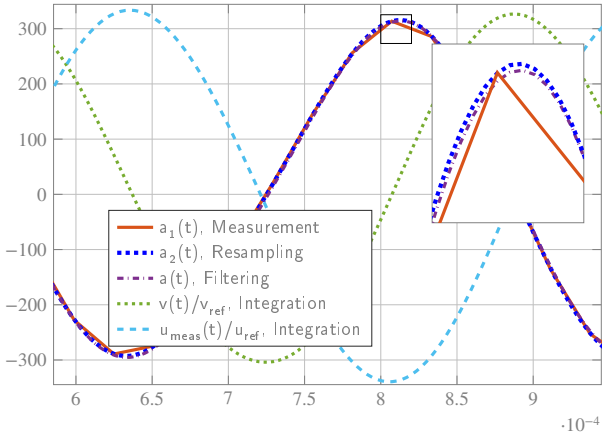


**Figure 5**: Comparison the different signals: measured acceleration $a_1(t)$, resampled acceleration $a_2(t)$, filtered acceleration $a(t)$, integrated velocity $v(t)$ and integrated displacement $u_{meas}(t)$.

### 3.6. Signal Filtering

The acceleration at the free end is measured by the piezoelectric sensor. The strain identification procedure (Fig. 9) includes filtering and integration of the acceleration signal in order to obtain the displacement then developing a dynamic vibrational inverse model.

The obtained data $a(t) = \frac{\partial^2 u_{meas}}{\partial t^2}$, $B(t)$ and $H(t)$ are analyzed in a way to draw a butterfly loop that characterizes the magneto-mechanical behavior. The acceleration is twice integrated giving the sheet's longitudinal displacement $u(t)$ at the accelerometer's position. We note that the displacement (and eventually the strain) is positioned in a way to have a minimum equal to zero.

$$u_{meas}(t) = \hat{u}(t, x = L) = \int \int a(t) dt^2 \tag{4}$$

The integration is performed numerically, but the initial signal $a(t)$ contains low frequency information due to the measurement's drift which induces divergence of the displacement signal (Fig. 7). The strategy consists in filtering

the signal by removing the low frequencies and keeping the high frequencies (High pass filtering). The cutoff frequency is 1.4 times the magnetic exciting frequency and 0.7 times the mechanical frequency. In fact, as explained in Section 5.1, the magnetic fundamental exciting frequency generates a mechanical response with a double frequency. Fig. 8 shows the integration results after filtering. Signal should not lose information after filtering; the less the energy is at low frequency before filtering, the less the losses are. However, the velocity and the displacement between the filtered and unfiltered signals are way different due to the integration even if the filtered acceleration changes slightly.

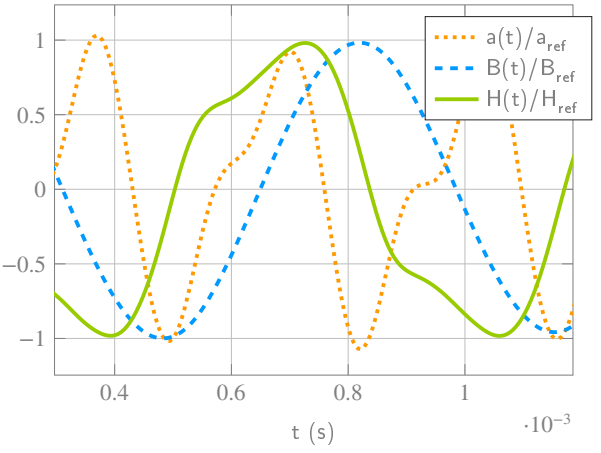


**Figure 6**: Time response of the three measured signals.

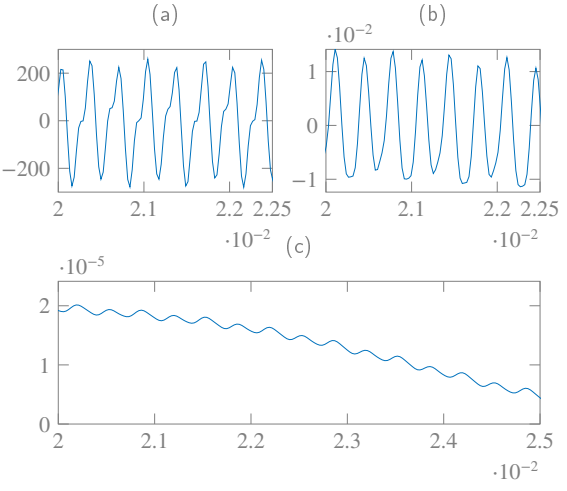


**Figure 7**: Acceleration integration without filtering: (a) acceleration (m.s$^{-2}$); (b) velocity (m.s$^{-1}$); (c) displacement (m), as function of time t (s).

## 4. Inverse Mechanical Model

### 4.1. Description and Modeling

We consider a magnetic sheet in the longitudinal direction. It is characterized by a modulus of elasticity $E = 160$ GPa, a density $\rho = 7,650$ kg.m$^{-3}$, a length 280 mm, a width $b = 30$ mm and a thickness $h = 0.26$ mm. The sample is fixed at one end and free at the other, and the equivalent free length is $L = 265$ mm. The sheet is uniformly magnetized within a specific region called magnetization zone determined by position $L_1$ and $L_2$ (Fig. 3). Furthermore, a uniform local magnetic strain $\epsilon_{ms}$, is locally generated, having a similar behavior of the thermal expansion. The considered

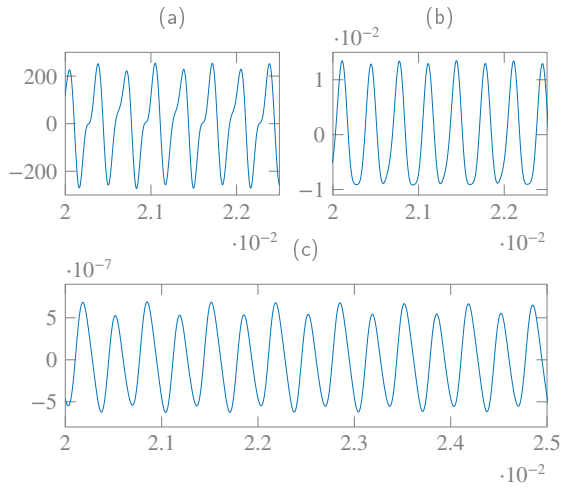


**Figure 8**: Acceleration integration with filtering: (a) acceleration (m.s$^{-2}$); (b) velocity (m.s$^{-1}$); (c) displacement (m), as function of time t (s).

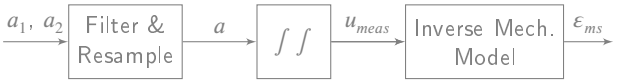


**Figure 9**: Identification of the local magnetostriction based on the acceleration measurements.

strain is unifomly applied in the magnetized length and is averaged in the cross section ($z-$direction). The stress $\sigma_{ms}$ that is equivalent to the magnetic strain is given by,

$$\varepsilon_{ms}(t) = \frac{\sigma_{ms}(t)}{E} \tag{5}$$

The stress is uniform along the magnetized length (between $L_1$ and $L_2$) and equal to zero in the region between 0 to $L_1$ and $L_2$ to $L$. An equivalent concentrated axial load $F_{ms} = -\frac{\partial \sigma_{ms}}{\partial x}$ is obtained at positions $L_1$ and $L_2$. As a result, the dynamic mechanical behavior of the fixed-free sample represented by the longitudinal displacement $\hat{u}(x,t)$ in the $x-$ direction is modeled by the following differential equation and boundary conditions [24],

$$\rho \frac{\partial^2 \hat{u}}{\partial t^2} + c\frac{\partial \hat{u}}{\partial t} = F_{ms} + E\frac{\partial^2 \hat{u}}{\partial x^2} \tag{6}$$

$$\hat{u}(0,t) = 0 \tag{7}$$

$$\frac{\partial \hat{u}}{\partial x}(L,t) = 0 \tag{8}$$

$c$ is a damping constant that represents the mechanical dissipation of the material (in kg/s).
We define $\varepsilon_a$ the apparent strain directly resulting from the displacement $\hat{u}(t)$ solution of Eq. (6).

$$\varepsilon_a(t) = \frac{\partial \hat{u}}{\partial x}(t) \tag{9}$$

It contains information concerning the magnetostriction, but also the inertia effect. It represents the apparent strain that is locally measured when using a strain gauge. In the case where the inertia effect is negligible compared to the stiffness, the apparent strain is equal to $\varepsilon_{ms}$. Furthermore, $\varepsilon_a$ describes the observed behavior related to vibrations and

noise due to the combination of the geometric conditions and the magneto-mechanical properties. Both $\varepsilon_a$ and $\varepsilon_{ms}$ are averaged through the cross section (z independent) but they are potentially x-dependent. However, the SST gives a uniform strain in the magnetized area through the $x$ direction which makes the identification of local magneto-mechanical properties easier.

## 4.2. Discretization

The sample is discretized using the 1D Finite Element Method (FEM) with quadratic elements. Combining Eq. (6) with the boundary conditions (Eqs. (7) and (8)), a dynamic system of $n$ equations with mass $\boldsymbol{M}$, damping $\boldsymbol{C}$ and stiffness $\boldsymbol{K}$ matrices and excitation vector $\varepsilon_{ms}\boldsymbol{f}$ is obtained. A discretized displacement vector $\boldsymbol{u}$ and a discretized acceleration vector $\ddot{\boldsymbol{u}}$:

$$\boldsymbol{M}\ddot{\boldsymbol{u}} + \boldsymbol{C}\dot{\boldsymbol{u}} + \boldsymbol{K}\boldsymbol{u} = \varepsilon_{ms}\boldsymbol{f} \tag{10}$$

The determination of the damping matrix $\boldsymbol{C}$ is performed in section 5.2.
From a static point of view, using Eq. (10), one gets the static displacement vector $\boldsymbol{u_s}$ from the static excitation vector $\boldsymbol{f_s}$ ($\boldsymbol{u_s} = \varepsilon_{ms}\boldsymbol{K}^{-1}.\boldsymbol{f_s}$). The shape of the deformed sample and its deformation are illustrated in Fig. 10. Three regions are distinguished: between the clamping and the position $L_1$ no deformation or displacement are shown, between $L_1$ and $L_2$ the displacement linearly increases and the deformation is uniform, and in the free region a constant displacement is observed with no deformation. However, for the dynamic behavior, the shape function is modified, specially when the study is near the resonance as explained in section 5.3. Considering a uniform strain and a linear displacement,

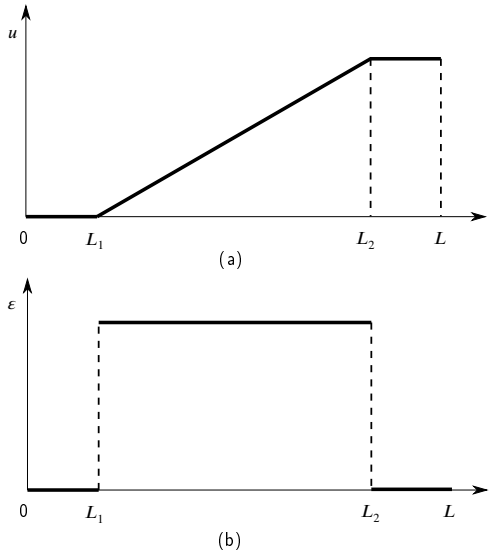


**Figure 10**: Displacement and strain versus sheet's length under static conditions.

the apparent strain defined in Eq. (9) can be expressed as a function of the measured displacement $u_{meas}(t)$ in the magnetized length by,

$$\varepsilon_a(t) = \frac{\partial \hat{u}}{\partial x}(t) = \frac{\Delta u}{\Delta L} = \frac{u_{meas}(t)}{L_2 - L_1} \tag{11}$$

The experimental measurement gives the displacement at the free end of the sample. Hence, the last element of the vectors $\boldsymbol{u}$, $\dot{\boldsymbol{u}}$ and $\ddot{\boldsymbol{u}}$ is known and it corresponds to the measured acceleration, the integrated velocity and the integrated displacement at the free end. The other $n-1$ components of the vectors and the equivalent strain $\varepsilon_{ms}$ are unknown; $n$ equations and $n$ unknowns are obtained. The identification of the unknowns is performed by developing an inverse solving method. We split vertically the mass, the damping and stiffness matrices in two parts: $\boldsymbol{M_1}$, $\boldsymbol{C_1}$ and $\boldsymbol{K_1}$ with $n \times n-1$ dimensions and $\boldsymbol{M_2}$, $\boldsymbol{C_2}$ and $\boldsymbol{K_2}$ with $n \times 1$ dimensions.

$$\boldsymbol{M} = \left[\ \boldsymbol{M_1} \mid \boldsymbol{M_2}\ \right]_{n\times n} \tag{12}$$

$$\boldsymbol{C} = \left[ \begin{array}{c|c} \boldsymbol{C_1} & \boldsymbol{C_2} \end{array} \right]_{n\times n} \tag{13}$$

$$\boldsymbol{K} = \left[ \begin{array}{c|c} \boldsymbol{K_1} & \boldsymbol{K_2} \end{array} \right]_{n\times n} \tag{14}$$

In a similar way, we split horizontally the displacement, the velocity and the acceleration vectors into $\boldsymbol{u_1}$, $\dot{\boldsymbol{u}}_{\boldsymbol{1}}$ and $\ddot{\boldsymbol{u}}_{\boldsymbol{1}}$ the unknown components of dimensions $n-1\times 1$ and $u_{meas}$, $\dot{u}_{meas}$ and $\ddot{u}_{meas}$ the known components of dimension $1\times 1$:

$$\ddot{\boldsymbol{u}} = \left[ \frac{\ddot{\boldsymbol{u}}_{\boldsymbol{1}}}{\ddot{u}_{meas}} \right]_{n\times 1} \tag{15}$$

$$\dot{\boldsymbol{u}} = \left[ \frac{\dot{\boldsymbol{u}}_{\boldsymbol{1}}}{\dot{u}_{meas}} \right]_{n\times 1} \tag{16}$$

$$\boldsymbol{u} = \left[ \frac{\boldsymbol{u_1}}{u_{meas}} \right]_{n\times 1} \tag{17}$$

The following $n\times n$ system of equation is obtained:

$$\boldsymbol{M_1}\ddot{\boldsymbol{u}}_{\boldsymbol{1}} + \boldsymbol{C_1}\dot{\boldsymbol{u}}_{\boldsymbol{1}} + \boldsymbol{K_1}\boldsymbol{u_1} - \varepsilon_{ms}\boldsymbol{f} = -\boldsymbol{M_2}\ddot{u}_{meas} - \boldsymbol{C_2}\dot{u}_{meas} - \boldsymbol{K_2}u_{meas} \tag{18}$$

$$\overline{\boldsymbol{M}}\ddot{\overline{\boldsymbol{u}}} + \overline{\boldsymbol{C}}\dot{\overline{\boldsymbol{u}}} + \overline{\boldsymbol{K}}\overline{\boldsymbol{u}} = \overline{F} \tag{19}$$

where $\overline{F} = -\boldsymbol{M_2}\ddot{u}_{meas} - \boldsymbol{C_2}\dot{u}_{meas} - \boldsymbol{K_2}u_{meas}$, $\overline{M} = \left[ \begin{array}{c|c} \boldsymbol{M_1} & \boldsymbol{0}_{n\times 1} \end{array} \right]$, $\overline{C} = \left[ \begin{array}{c|c} \boldsymbol{C_1} & \boldsymbol{0}_{n\times 1} \end{array} \right]$, $\overline{K} = \left[ \begin{array}{c|c} \boldsymbol{K_1} & -\boldsymbol{f} \end{array} \right]$ and $\overline{\boldsymbol{u}} = \left[ \frac{\boldsymbol{u_1}}{\varepsilon_{ms}} \right]$

Eq. (19) is time discretized with a time step $\Delta t$ using a four-point backward difference approximation of the Taylor series development for the second derivative (acceleration) and a three-point backward difference approximation for the first derivative (velocity). The displacement, the velocity and acceleration unknown vectors are then time discretized by:

$$\ddot{\overline{\boldsymbol{u}}}(t_n) = \frac{1}{\Delta t^2}[2\overline{\boldsymbol{u}}(t_n) - 5\overline{\boldsymbol{u}}(t_{n-1}) + 4\overline{\boldsymbol{u}}(t_{n-2}) - \overline{\boldsymbol{u}}(t_{n-3})] \tag{20}$$

$$\dot{\overline{\boldsymbol{u}}}(t_n) = \frac{1}{2\Delta t}[3\overline{\boldsymbol{u}}(t_n) - 4\overline{\boldsymbol{u}}(t_{n-1}) + \overline{\boldsymbol{u}}(t_{n-2})] \tag{21}$$

Combining Eqs. (19) and (21), one gets:

$$\left( \frac{2}{\Delta t^2}\overline{\boldsymbol{M}} + \frac{3}{2\Delta t}\overline{\boldsymbol{C}} + \overline{\boldsymbol{K}} \right) \overline{\boldsymbol{u}}(t_n) = \overline{F} + \frac{5\overline{\boldsymbol{u}}(t_{n-1}) - 4\overline{\boldsymbol{u}}(t_{n-2}) + \overline{\boldsymbol{u}}(t_{n-3})}{\Delta t^2}\overline{\boldsymbol{M}} + \frac{4\overline{\boldsymbol{u}}(t_{n-1}) - \overline{\boldsymbol{u}}(t_{n-2})}{2\Delta t}\overline{\boldsymbol{C}} \tag{22}$$

An incremental linear system of $n$ equations $\tilde{u}(t)$ and $n$ unknowns is obtained as follows:

$$\overline{\boldsymbol{u}}(t) = \boldsymbol{A}^{-1}\boldsymbol{B}(t_{n-1}, t_{n-2}, t_{n-3}) \tag{23}$$

with $\boldsymbol{A} = \frac{2}{\Delta t^2}\overline{\boldsymbol{M}} + \frac{3}{2\Delta t}\overline{\boldsymbol{C}} + \overline{\boldsymbol{K}}$ and $\boldsymbol{B} = \overline{F} + \frac{5\overline{\boldsymbol{u}}(t_{n-1}) - 4\overline{\boldsymbol{u}}(t_{n-2}) + \overline{\boldsymbol{u}}(t_{n-3})}{\Delta t^2}\overline{\boldsymbol{M}} + \frac{4\overline{\boldsymbol{u}}(t_{n-1}) - \overline{\boldsymbol{u}}(t_{n-2})}{2\Delta t}\overline{\boldsymbol{C}}$

The last term of solved time vector $\overline{\boldsymbol{u}}(t)$ corresponds to $\varepsilon_{ms}(t)$, taking into consideration the geometric and mechanical properties and the boundary conditions in the SST. The presented inverse mechanical modeling is developed using Matlab.

# 5. Modal analysis

## 5.1. Natural, Magnetic and Mechanical Frequencies

The considered magnetic sheet is clamped at one end and free at the other. Therefore, the $i^{th}$ theoretical natural frequency of the structure for this mechanical configuration is given by [22]:

$$f_i = \frac{(2i+1)}{4L}\sqrt{\frac{E}{\rho}} \tag{24}$$

Furthermore, the natural frequencies vector can also be calculated using the derived mass and stiffness matrices. The eigenvectors matrix $\mathbf{\Phi} =$ with $\boldsymbol{\phi}_i$ vectors and the eigenvalues diagonal matrix $\mathbf{\Omega} = \text{diag}(\omega_i)$ are obtained using the following classical eigen-equation:

$$(-\omega_i^2 \boldsymbol{M} + \boldsymbol{K})\boldsymbol{\phi}_i = 0 \tag{25}$$

The natural frequency is obtained by calculating the eigenvalues of Eq. (25):

$$\mathbf{\Omega^2} = eig(\boldsymbol{M^{-1}}.\boldsymbol{K}) \tag{26}$$

$$f_i = \frac{\omega_i}{2\pi} \tag{27}$$

The first 4 natural frequencies in the studied case are presented in Table 2. Identical results are obtained using Eq. (24) and (26). On the other hand, we define $f_{mag}$ the exciting fundamental frequency of the induction. The generated

**Table 2**
Longitudinal vibration's natural frequencies of the magnetic sheet in the studied setup.

| Mode | 1 | 2 | 3 | 4 |
|---|---|---|---|---|
| Frequency (Hz) | 4,314 | 12,943 | 21,572 | 30,201 |

mechanical response is performed with a fundamental mechanical frequency $f_{mech}$ equal the double of $f_{mag}$ frequency. In fact, magnetic forces, stresses or strains are equal to a linear combination of squared induction powers $|\varepsilon_{ms}| = \sum_{i=1}^{n} \alpha_i ||B^{2i}||$ [1]. We note that due to the magnetic non-linearity ($n > 1$), the mechanical response can present next to the fundamental frequency $f_{mech}$, some harmonics ($2f_{mech}, 3f_{mech}$...).
In this experimental setup, when applying a magnetic frequency of $f_{mag} = 2,100$ Hz corresponding to the mechanical frequency $f_{mech} = 4,200$ Hz that is close to the fundamental natural frequency (of 4,300 Hz), a peak is obtained for the apparent strain $\varepsilon_a$ as shown in Fig. 17. This resonance phenomenon appears for different induction amplitudes as illustrated in Fig. 11.

## 5.2. Damping Effect Identification

Once the eigenvectors and the eigenvalues are calculated, and using a modal transformation, the diagonal matrices $\boldsymbol{\mu}$, $\boldsymbol{\mu\Omega^2}$ and $2\boldsymbol{\mu\xi\Omega}$ are respectively defined as [25]:
Modal mass matrix:

$$\boldsymbol{\mu} = \text{diag}(\mu_i) = \mathbf{\Phi}^T \boldsymbol{M}\mathbf{\Phi} \tag{28}$$

Modal stiffness matrix:

$$\boldsymbol{\mu\Omega^2} = \text{diag}(\mu_i\omega_i^2) = \mathbf{\Phi}^T \boldsymbol{K}\mathbf{\Phi} \tag{29}$$

Modal damping matrix:

$$2\boldsymbol{\mu\xi\Omega} = \text{diag}(2\xi_i\mu_i\omega_i) = \mathbf{\Phi}^T \boldsymbol{C}\mathbf{\Phi} \tag{30}$$

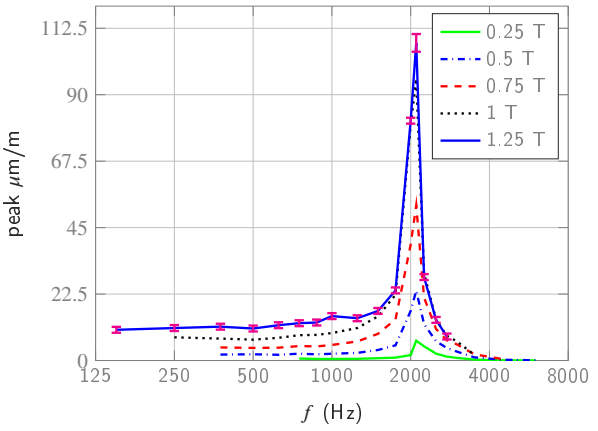


**Figure 11**: Peak-To-Peak analysis of the apparent strain with respect to the applied frequency.

$\boldsymbol{\mu}$, $\boldsymbol{\Omega}$ are already known, $\boldsymbol{\xi} = \text{diag}(\xi_i)$ is the damping ratios matrix that is experimentally identified. Therefore the damping matrix $\boldsymbol{C}$ can be calculated:

$$\boldsymbol{C} = 2\boldsymbol{\Phi}^{T^{-1}}\boldsymbol{\mu}\boldsymbol{\xi}\boldsymbol{\Omega}\boldsymbol{\Phi}^{-1} \tag{31}$$

The identification of the damping ratio is obtained experimentally by magnetizing the clamped-free plate. At the moment where the magnetic field signal is cut, the excitation is removed; an underdamped oscillatory response is obtained (Fig. 12). The damping ratio $\xi_1$ at the first mode is identified by measuring the overshoots of the response. Considering an initial overshoot of $y_i$ and a final overshoot of $y_f$ after $N_c$ cycles, a logarithmic decrement $\delta$ is defined as follows:

$$\delta = \frac{1}{N_c}\ln\left(\frac{y_i}{y_f}\right) \tag{32}$$

The damping ratio for the first mode is then given by:

$$\xi_1 = \frac{\delta}{\sqrt{(2\pi)^2 + \delta^2}} \tag{33}$$

It is shown from the calculation that the first mode damping ratio $\xi_1$ is between 0.025-0.035, which is the damping ratio range for electrical steels. Considering this value for estimation of the damping matrix in Eq. (31), we notice that the damping effect, even at high frequencies (up to 6,000 Hz), is still negligible in the identification of $\varepsilon_{ms}$ and the identification discrepancy with4 and without damping consideration is equal to 1% in average (Fig. 13). Therefore, the analysis can be performed without taking into consideration the damping matrix when dealing with electrical steels.

### 5.3. Frequency Dependent Shape function

Taking into account the different frequencies presented in the previous section, we consider several input magnetic frequencies that excite the structure with mechanical frequency lower, higher and near the resonance. Applying Eq. (10) for a random strain $\varepsilon_{ms}$ and for different magnetic frequencies, the length dependent displacement at a random time is obtained in Fig. 14 showing that the inclusion of the inertia effect modifies the shape function obtained in Fig. 10. Furthermore, at low frequency (500 Hz), the inertia effect is negligible which leads to the same shape function of the static case (Fig. 10). For a higher frequency (1,050 Hz), the shape function is distorted but still presents a singular transition at $L_1$ and $L_2$ with lower effect. At the resonance, the shape function looks more continuous. At higher frequencies (3,000 Hz), the shape function is totally modified showing a decreasing displacement in the magnetized region due to the inertia effect that becomes more important than the stiffness effect.

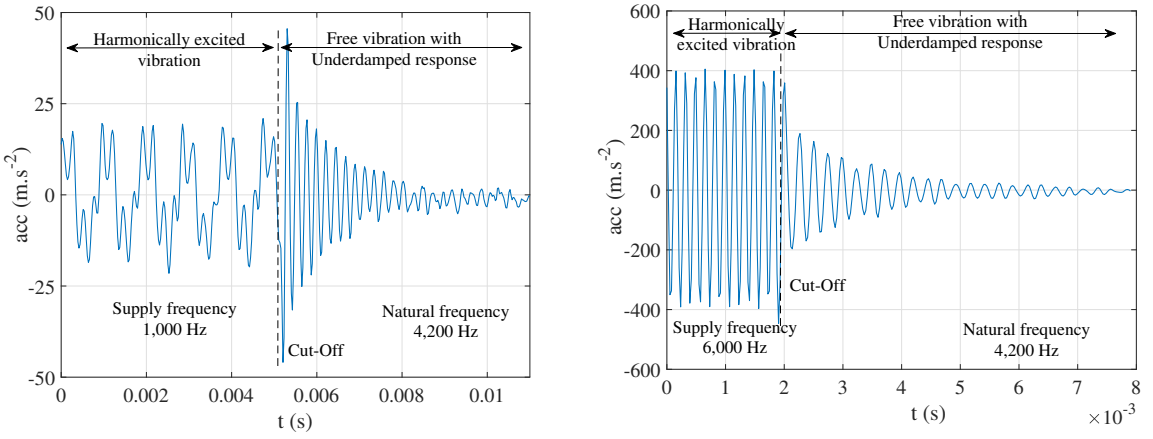


**Figure 12**: Acceleration response before and after cut-off (a) 1 T, 500 Hz; (b) 1 T, 3,000 Hz.

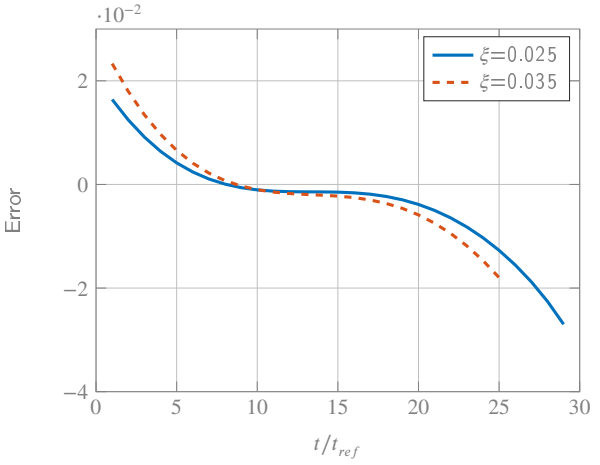


**Figure 13**: Relative difference between the identified strain $\varepsilon_{ms}$ at $\xi = 0.025 - 0.035$ (damping) and at $\xi = 0$ (no damping) for one cycle of 1,500 Hz and at 1 T.

## 6. Results

Different magnetic excitation magnitudes ($B_m$ =0.25 T, 0.5 T, 0.75 T, 1 T, 1.25 T and 1.5 T) and magnetic excitation frequencies ($f_{mag}$ = 500 Hz, 1,050 Hz, 1,500 Hz, 2,100 Hz, 3,000 Hz) are considered. Frequencies are chosen a way to cover a large region of the frequency spectrum with respect to the resonance frequency. 500 Hz and 1,500 Hz are random magnetic frequencies lower than the resonance magnetic frequency, 2,100 Hz is close to resonance and 3,000 Hz is a random value chosen higher than the resonance frequency. As for 1,050 Hz frequency, it corresponds to the quarter of the resonance frequency.

**Before the resonance ($f_{mag}$ = 500 Hz, 1,500 Hz)**

We first consider magnetic excitations of $f_{mag}$ = 500 Hz and 1,500 Hz magnetic excitation. The identification technique developed above gives the magnetic induced strain and the apparent strain. Coupling results are illustrated using a $\varepsilon = f(B)$ by removing the time variable; a butterfly loop is obtained showing the amplitude ratio between the mechanical and magnetic properties, the time delay due to the loop's width, and a parabolic shape due to the squared-relation. Figs. 15 and 16 show respectively the butterfly loops obtained for $f_{mag}$ = 500 Hz and $f_{mag}$ = 1,500 Hz using both strains $\varepsilon_{ms}$ and $\varepsilon_a$ calculated in Eqs. (23) and (11). At 500 Hz, it is noticed that $\varepsilon_{ms}$ is almost equal to $\varepsilon_a$. In this case, the inertia effect is negligible compared to the stiffness and the excitating mechanical frequency ($f_{mech}$ = 1,000

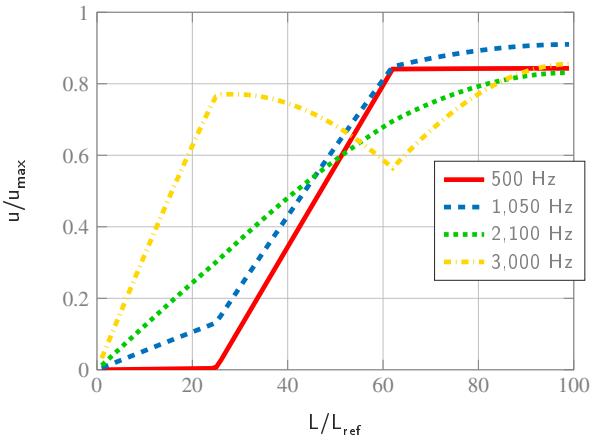


**Figure 14**: Displacement shape function for different exciting frequencies.

Hz) is much lower than the natural frequency ($f_1 = 4{,}300$ Hz). Contrariwise at $f_{mag} = 1{,}500$ Hz, $\varepsilon_{ms}$ is much lower than $\varepsilon_a$ due to the more effective inertia for a mechanical frequency ($f_{mech} = 3{,}000$ Hz) closer to resonance. On the other hand, it is noticed that the higher the induction is, the higher the strain and the time delay are. For an induction of 0.75 T, we reach an amplitude of $\varepsilon_a$ around 8 $\mu$m/m and of $\varepsilon_{ms}$ around 4 $\mu$m/m, and for an induction of 1.25 T, $\varepsilon_a$ is around 13 $\mu$m/m and $\varepsilon_{ms}$ around 7 $\mu$m/m.

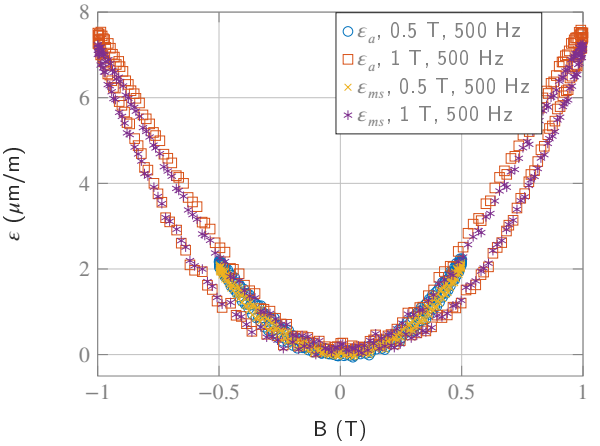


**Figure 15**: Butterfly loop at $f_{mag} = 500$ Hz of the apparent strain $\varepsilon_a$ (with the inertia effect), and the magnetic induced strain $\varepsilon_{ms}$ (removing the inertia effect) ($\pm 5\%$ error).

**Near the resonance ($f_{mag} = 2{,}100$ Hz)**
The mechanical resonance occurs around 4,300 Hz corresponding to a 2,150 Hz frequency. A 2,100 Hz induction frequency is then considered for measurement. It is clearly noticed that the deformation amplitude highly increases at $f_{mag} = 2{,}100$ Hz in comparison with the other frequencies as shown in the butterfly loops of Fig. 17 and in the Peak-To-Peak analysis of Fig. 11. We must avoid this frequency when measuring and identifying the magnetic strain because the model's accuracy decreases at the critical resonance point.

**After the resonance ($f_{mag} = 3{,}000$ Hz)**
Fig. 18 plots $\varepsilon_a$ and $\varepsilon_{ms}$ at $f_{mag} = 3{,}000$ Hz, corresponding to $f_{mech}$ =6,000 Hz that is higher than the resonance frequency. $\varepsilon_a$ shows a negative delay with the induction due to the inertia dominance. Removing the inertia effect, the

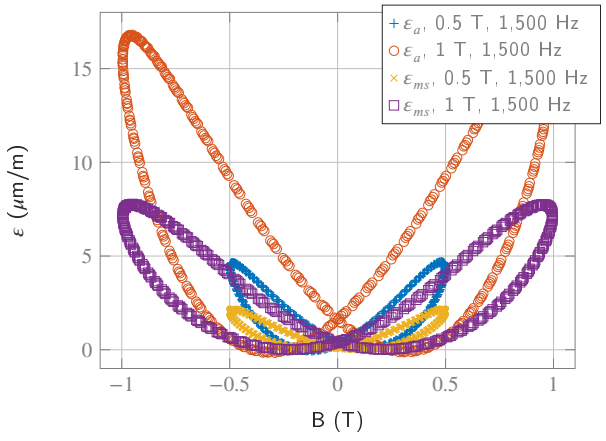


**Figure 16**: Butterfly loop at $f_{mag}$ = 1,500 Hz of the apparent strain $\varepsilon_a$ (with the inertia effect), and the magnetic induced $\varepsilon_{ms}$ (removing the inertia effect) (±5% error).

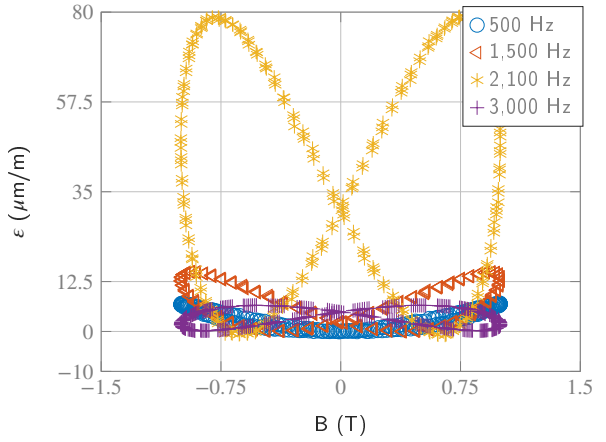


**Figure 17**: Butterfly loop comparison at 1 T between the apparent strain for $f_{mag}$ = 1,050 Hz, 1,500 Hz and 2,100 Hz (±5% error).

real $\varepsilon_{ms}$ is obtained showing a positive delay between the magneto-mechanical variables. This delay is relatively high due to the high frequency.

**At ($f_{mag}$ = 1,050 Hz)**

Magneto-mechanical measurements at 1,050 Hz corresponding to the quarter of the mechanical resonance frequency are performed. The butterfly loop presented in Fig. 19 illustrates the $\varepsilon_a$ at $f_{mag}$ =1,050 Hz with a different butterfly shape. Next to the fundamental frequency of $f_{mech}$ = 2,100 Hz, a harmonic frequency of 4,200 Hz is observed (Fig. 20) for the mechanical response. In fact, the presence of a 3,150 Hz harmonic with a small contribution in the magnetic field (Fig. 22) combined with the frequency of 1,050 Hz observed in the fundamental of the induction and the magnetic field (Figs. 22 and 23) generates a fundamental mechanical frequency of 2,100 Hz, but also a 4,200 Hz mechanical harmonic similar the energy spectrum shown in Fig. 21. In fact, although the average induction contains only fundamental frequency of 1,050 Hz (Fig. 23), but locally, the induction distribution profile contains harmonics due to the non-linearity provided by the magnetic field [23]. Therefore, magnetic strain harmonics are sensitive to this non-linearity generating mechanical frequencies with the sum of the different magnetic frequencies combinations (1,050 Hz and 3,150 Hz magnetic → 2,100 Hz, 4,200 Hz and 6,300 Hz mechanical). Furthermore, the 4,200 Hz frequency contribution is amplified due to the mechanical resonance at 4,300 Hz. Therefore, the butterfly loop shape of the apparent strain is different and internal loops are observed because of the amplification of the 4,200 Hz harmonic

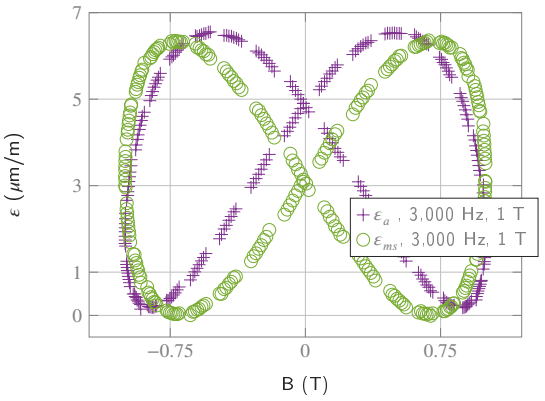


**Figure 18**: Butterfly loop at $f_{mag}$ = 3,000 Hz of $\epsilon_a$ and $\epsilon_{ms}$ (±10% error).

in Fig. 19. However, when applying the inverse model to remove the inertia effect, magnetic strain $\epsilon_{ms}$ is restituted as shown in Fig. 24 and the 4,200 Hz effect is reduced.

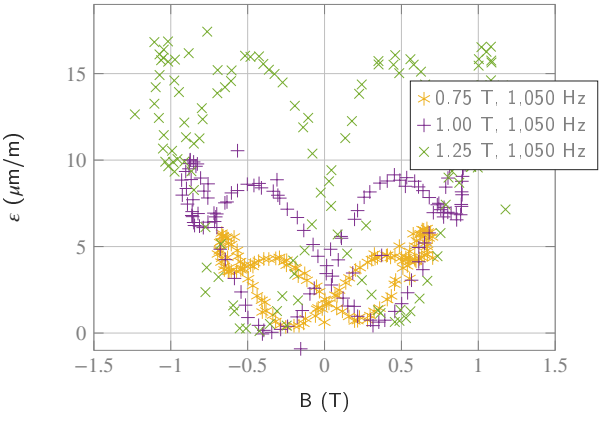


**Figure 19**: Butterfly loop of the apparent magnetostriction $\epsilon_a$ at $f_{mag}$ = 1,050 Hz (±5% error).

**Frequency Dependence Magnetostriction**

Fig. 24 illustrates $\epsilon_{ms}$ for 500 Hz, 1,050 Hz and 1,500 Hz and shows that the higher the frequency the larger the loop's width. In fact, the time delay between the mechanical and the magnetic signals increases with the frequency. This is due to the presence of a damping property between the magnetization and the deformation that generates phase shifting between both signals [14]. This is a magneto-mechanical delay in the magnetic structure constituted of magnetic domains separated by magnetic walls. In fact, the presence of eddy current around the walls generates a viscous damping force [26] responsible of the mechanical dissipation and eventually the time delay between the magnetization and the magnetic strain.

## 7. Conclusion

Measurement and identification of the magnetic induced strain in electrical steels have been developed using a non-desctructive technique. It is based on measurement using a piezoelectric accelerometer and an inverse vibrational model that identifies the magneto-mechanical property. The one-dimensional vibrational model has been used to calculate the magnetic strain based on the acceleration measurements at the end of the magnetic sheet magnetized inside the Single Sheet Tester. Frequency analysis is performed showing the effect of resonance frequency on the magneto-mechanical dynamic behavior. We also distinguish between the apparent strain dependent on the geometric

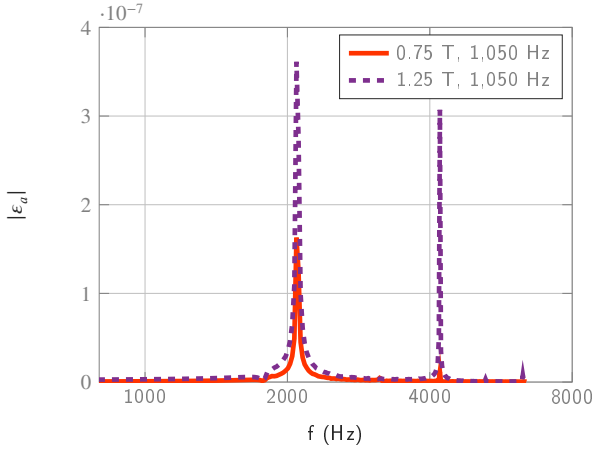


**Figure 20**: Frequency spectrum of the apparent magnetostriction $\varepsilon_a$ when applying a magnetic excitation of $f_{mag}$ = 1,050 Hz.

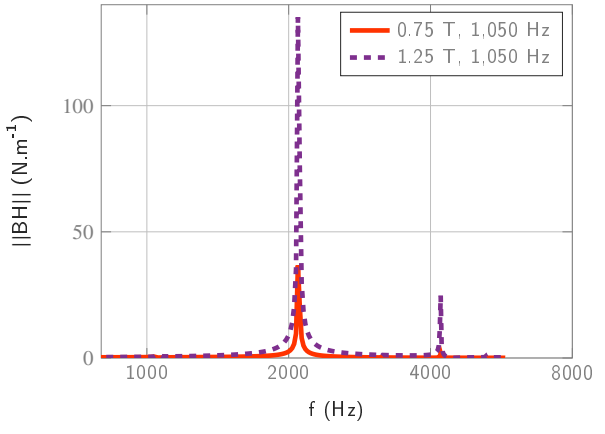


**Figure 21**: Magnetic energy density spectrum with an excitation of $f_{mag}$ = 1,050 Hz.

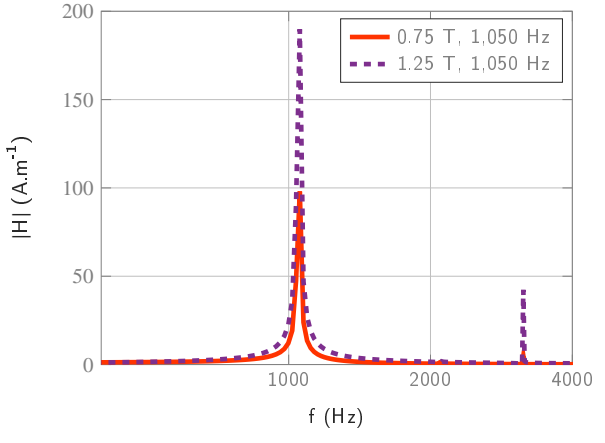


**Figure 22**: Magnetic field spectrum with an excitation of $f_{mag}$ = 1,050 Hz.

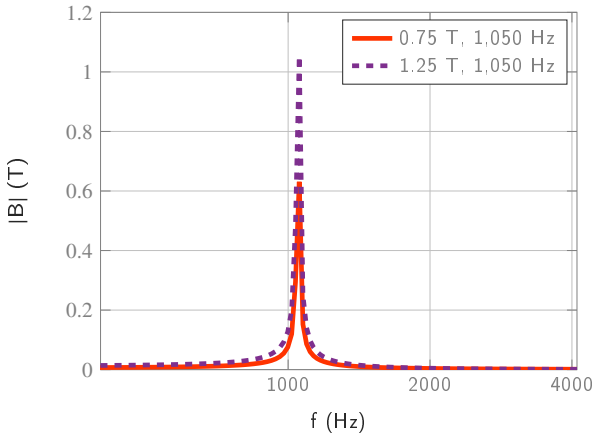


**Figure 23**: Induction spectrum with an excitation of $f_{mag}$ = 1,050 Hz.

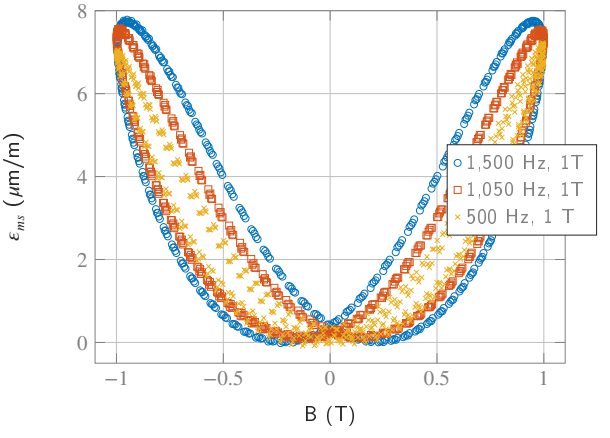


**Figure 24**: Comparison of the magnetic strain between 500 Hz, 1,050 Hz and 1,500 Hz (±5% error).

and mechanical conditions and the magnetic induced strain, a characteristic of the material. The developed technique is one important tool for analyzing the physical properties that describe the magneto-mechanical coupled behavior of electrical steels. It is also a non-destructive technique that measures the strain before and after a certain treatment of the same sample. This is a powerful technique for the identification and the improvement of the magneto-mechanical behavior.

## Acknowlegment

This work was carried out within the frame of the project ESSIAL, funding from the European Union's Horizon 2020, research and innovation program under grant agreement No 766437.

## References

[1] D. Singh U. Aydin, P. Rasilo, A. Lehikoinen, A. Belahcen, and A. Arkkio. Coupled Magneto-Mechanical Analysis of Iron Sheets Under Biaxial Stress. (52(3)), 2015.

[2] S. Sathyan, A. Belahcen, A. Lehikoinen, U. Aydin, and F. Boxberg. Investigation of the causes behind the vibrations of a highspeed solid-rotor induction motor. *Journal of Sound and Vibration*, 463:114976, 2019.

[3] J. Melkebeek T. Hilgert, L. Vandevelde. Comparison of Magnetostriction Models for Use in Calculations of Vibrations in Magnetic Cores. (44(6)):874–877, 2008.

[4] R. McConnell O. Mohammed, T. Calvert. A model for magnetostriction in coupled nonlinear finite element magneto-elastic problems in electrical machines. pages 728–735, 1999.

[5] K. Hameyer K. Delaere, R. Belmans, W. Heylen, and P. Sas. Coupling of magnetic and vibrational modal analysis using local forces. pages 417–422, 1999.

[6] A. Kameari H. Ebrahimi, Y. Gao, H. Dozono, and K. Muramatsu. Coupled Magneto-Mechanical Analysis Considering Permeability Variation by Stress Due to Both Magnetostriction and Electromagnetism. (49(5)):1621–1624, 2013.

[7] Y. Qingxin Z. Xian, Z. Pengcheng, Z. Lihua, and Z. Xin. Numerical Estimation and Optimization of Vibration Noise due to Magnetostriction and Magnetic Forces for laminated Core Structure. 17th International Conference on Electrical Machines and Systems (ICEMS), Hangzhou, China, Oct. 22-25, 2014.

[8] J. M. Gillard F. Delince, A. Genon, H. Hedia, and A. Nicolet W. Legros. Numerical computation of the magnetostriction effect in ferromagnetic materials. (69(8)):5794–5796, 1991.

[9] P. Rasilo U. Aydin, F. Martin, D. Singh, L. Daniel, A. Belahcen, M. Rekik, O. Hubert, R. Kouhia, and A. Arkkio. Magneto-mechanical modeling of electical steel sheets. (439):82–90, 2017.

[10] K. A. Fonteyn. *Energy-based magneto-mechanical model for electrical steel sheets*. PhD thesis, Aalto University, School of Electronics, Communications and Automation, 2010.

[11] K. Fonteyn A. Belahcen, A. Hannukainen, and R. Kouhia. On numerical modeling of coupled magnetoelastic problem. pages 203–206. 21st Nordic Seminar on Computational Mechanics, Trondheim, Norja, 2008.

[12] K. Fonteyn, A. Belahcen, R. Kouhi, P. Rasilo, and A. Arkkio. FEM for Directly Coupled Magneto-Mechanical Phenomena in Electrical Machines. (46(8)):2923–2926, 2010.

[13] C. Mudivarthi, S. Datta, J. Atulasimha, A. B. Flatau, P. G. Evans, and M. J. Dapinod. Equivalence of magnetoelastic, elastic, and mechanical work energies with stress-induced anisotropy. *Behavior and Mechanics of Multifunctional and Composite Materials*, 6929:69291X–69291X–9, 2008.

[14] P. Anderson S. Somkun, A. Moses and P. Klimczyk. Magnetostriction anisotropy and rotational magnetostriction of nonoriented electrical steel. *IEEE Transactions on Magnetics*, 46(2):302–305, 2010.

[15] A. J. Moses S. Somkun and P. I. Anderson. Measurement and Modeling of 2-D Magnetostriction of Nonoriented Electrical Steel. (48(2)):711–714, 2012.

[16] A. J. Moses S. Somkun, P. Klimczyk and P. Anderson. Comparisons of ac magnetostriction of non-oriented electrical steels measured in epstein and disc samples. *Journal of Electrical Engineering*, 61(7/s):89–92, 2010.

[17] A. Moses S. Somkun and P. Anderson. Measurement and modeling of 2-d magnetostriction of nonoriented electrical steel. *IEEE Transactions on Magnetics*, 48:711–714, 2012.

[18] S. Gorji Ghalamestani, L. Vandevelde, J. Dirckx, and J. Melkebeek. *Magnetostriction strain measurement: heterodyne laser interferometry versus strain gauge technique*, pages 167–174. 01 2013.

[19] J.M. Chicharro A. Bayòn and F. Salazar. Simultaneous measurement of field dependence of elastic moduli by laser interferometry. *Journal of Magnetism and Magnetic Materials*, 219:229–235, 2000.

[20] A. Bayòn J.M. Chicharro and F. Salazar. Measurement of field-dependence elastic modulus and magnetomechanical coupling factor by optical heterodyne interferometry. *Journal of Magnetism and Magnetic Materials*, 202:465–472, 1999.

[21] P. Anderson P. Klimczyk, S. Somkun and A. J. Moses. Comparison of uniaxial and rotational magnetostriction of non-oriented and grain-oriented electrical steel. *Przeglad Elektrotechniczny*, 87(9):33–36, 2011.

[22] A. J. Moses T. P. P. Phway and D. C. Jiles. Frequency dependence of magnetostriction for magnetic actuators. *Journal of electrical engineering*, 55:7–10, 2004.

[23] E. Salloum, O. Maloberti, M. Nesser, S. Panier, and J. Dupuy. Identification and analysis of static and dynamic magnetization behavior sensitive to surface laser treatments within the electromagnetic field diffusion inside go sife electrical steels. *Journal of Magnetism and Magnetic Materials*, 503:166613, 2020.

[24] S. S. Rao. *Mechanical Vibrations*. Prentice Hall, 2004.

[25] A. Preumont. *Vibration Control of Active Structures, An Introduction, $3^{rd}$ Edition*. Springer, 2011.

[26] C.B. Lin J.L. Lee. The Magnetic Viscous Damping Effect on the Natural Frequency of a Beam Plate Subject to an In-Plane Magnetic Field. 77(1):011014, 2010.